J. Synchrotron Rad. (1995). **2**, 181–184

The Use of Imaging Plates in Electron-Density Mapping with Synchrotron X-rays

Robert Bolotovsky, Alex Darovsky, Vladimir Kezerashvili and Philip Coppens

Department of Chemistry, Natural Sciences and Mathematics Complex, State University of New York at Buffalo, Buffalo, NY 14260-3000, USA

(*Received 10 April 1995; accepted 10 May 1995*)

Imaging-plate synchrotron data have been applied in the charge-density analyses of sodium nitroprusside and hexaamminechromium(III) hexacyanochromate(III), collected at 100 and 50 K, respectively, and photons of wavelengths 0.656 and 0.394 Å at the SUNY X3 beamline at NSLS. The electron-density maps show good agreement between chemically equivalent sections, while the multipole aspherical atom refinements lead to chemically reasonable population parameters, with trends reproduced in the available theoretical calculations. The results indicate that the time required for charge-density mapping with diffraction data can be greatly reduced by the application of the new technology.

Keywords: imaging plates; seed-skewness method; electron density.

1. Introduction

Whilst the use of area detectors is revolutionizing macromolecular data collection, it also has the potential of significantly reducing data-collection time in small-unit-cell structure determination. During the past year imaging plates have been routinely used to collect low-temperature data for structure determination at the SUNY X3 beamline at the National Synchrotron Light Source (NSLS) at Brookhaven National Laboratory (BNL). Structures analyzed include bis(4-bromophenyl)-61,61-diyl methanofullerene C_{60} (Iversen, Bolotovsky, Darovsky & Coppens, 1995) and $CuGe_2S_5.(C_2H_5)_4N$ (Tan, Darovsky & Parise, 1995). The usefulness of imaging plates in (room-temperature) small-moiety crystallography has also been pointed out by Grochowski, Serda, Wilson & Dauter (1994).

We report here that low-temperature imaging-plate data obtained with the seed-skewness method are of a quality adequate for charge-density analysis, for which requirements are more stringent than in conventional structure analysis. As the use of area detectors dramatically shortens data-collection time, they offer the possibility for more routine application of charge-density analysis in molecular and solid-state research.

As parasitic scattering by cryostat vacuum chambers is a problem with area detectors, which do not allow use of a diffracted beam collimator, we have constructed an antiscatter device with a collimator/radiation shield in front, and a backstop behind the crystal, both within the vacuum chamber and kept stationary on φ-rotation (Darovsky, Bolotovsky & Coppens, 1994). We have also developed methods for accurate image analysis using a seed-skewness algorithm (Bolotovsky, White, Darovsky & Coppens, 1995).

In the case of synchrotron radiation, rapid data collection and the use of repeated oscillations for each recording minimize the effect of photon-beam instabilities. Though it is our experience that the use of sequential counting techniques requires very frequent measurement of standard reflections at the bending-magnet X3 beamline, we have encountered no comparable difficulties when using imaging plates with the oscillation method.

2. Experimental

Low-temperature data were collected at the fixed-angle sideways X3A1 beamline at NSLS at BNL (Darovsky, Meshkovsky & Coppens, 1995), using photons of wavelengths 0.656 and 0.394 Å, obtained with Si(111) and Si(220) monochromating crystals, respectively. A Displex CT201 cryostat (Graafsma, Sagerman & Coppens, 1991) was used for cooling. Data on $Na_2[Fe(NO)CN_5].2H_2O$ (sodium nitroprusside dihydrate, SNP) were collected at λ = 0.656 Å and ~100 K, and on $[Cr(NH_3)_6][Cr(CN)_6]$ [hexaamminechromium(III) hexacyanochromate(III)], at ~50 K and 0.394 Å. The difference in temperature between the two experiments is mainly due to the use of one heat shield in the former and two heat shields in the latter experiment. In all studies 8° ω oscillations were used with 2° overlap between successive plates for a total range of 180°. The 2θ arm to which the imaging plate holder was attached was moved to collect high-order data. The 20 × 25 cm plates were read with a Fuji BAS2000 scanner. All measurements were repeated, and the plates from the second measurement read with a lower sensitivity of the scanner, to compensate for the limited dynamic range (10^4) of the scanner. Space-group information and details on the data collection are given in Tables 1 and 2.

3. Data reduction

Data integration was performed with the program *HIPPO*, which is based on the seed-skewness method (Bolotovsky

Table 1
Experimental data on sodium nitroprusside.

Space group	*Pnnm*
Temperature (K)	~100
Cell dimensions (Å)	a = 6.132 (2)
	b = 11.842 (2)
	c = 15.533 (3)
V (Å^3)	1128.0 (4)
Z	4
D_x (g cm^{-3})	1.754
Absorption coefficient (cm^{-1})	14.12
Crystal dimensions (mm)	0.2 × 0.5 × 0.6
Radiation wavelength (Å)	0.656
$(\sin\theta/\lambda)_{min}$–$(\sin\theta/\lambda)_{max}$ (Å^{-1})*	0.118–1.063
hkl range	–6, 8; –25, 14; –33, 29
Number of reflections measured	10 224
Number of unique reflections with $F > 3\sigma(F)$	2230
Merging R factor	0.020
Summary of least-squares results	
Number of variables	148
$R(F)$	0.0159
$wR(F)$	0.0202
$R(F^2)$	0.0300
$wR(F^2)$	0.0381
S	1.43

* For reflections with $F > 3\sigma(F)$.

Table 2
Experimental data on hexaamminechromium(III) hexacyanochromate(III).

Space group	$R\bar{3}$
Temperature (K)	~50
Cell dimensions (Å, °)	a = 7.4010 (5)
	α = 98.04 (2)
V (Å^3)	392.18 (8)
Z	1
D_x (g cm^{-3})	1.446
Absorption coefficient (cm^{-1})	2.34
Crystal dimensions (mm)	0.05 × 0.05 × 0.1
Radiation wavelength (Å)	0.394
$(\sin\theta/\lambda)_{min}$–$(\sin\theta/\lambda)_{max}$ (Å^{-1})*	0.207–1.552
hkl range	2, 22; –19, 14; –18, 19
Number of reflections measured	8018
Number of unique reflections with $F > 3\sigma(F)$	3445
Merging R factor	0.027
Summary of least-squares results	
Number of variables	77
$R(F)$	0.0228
$wR(F)$	0.0185
$R(F^2)$	0.0305
$wR(F^2)$	0.0271
S	0.69

* For reflections with $F > 3\sigma(F)$.

et al., 1995). Crystallographic data and experimental details are summarized in Tables 1 and 2. Because of the proximity of the backstop to the crystal, very low order reflections could not be collected. This led to a loss of eight unique low-order reflections for SNP. For the shorter-wavelength data set on the chromium complex, the corresponding number was 20. No absorption correction was applied to the hexaamminechromium(III) hexacyanochromate(III) short-wavelength data (μ = 2.34 cm^{-1}, maximum dimension of the sample 100 μm).

Table 3
Merging R factors for hexaamminechromium(III) hexacyanochromate(III).

(*a*) As a function of the F^2 range (arbitrary scale).

Interval	R	Number of terms	Number of means
100.0 < F^2 < 300.0	0.1037	129	58
300.0 < F^2 < 1000.0	0.0991	1613	680
1000.0 < F^2 < 3000.0	0.0623	2013	829
3000.0 < F^2 < 10000.0	0.0339	1718	678
10000.0 < F^2 < 30000.0	0.0216	911	351
30000.0 < F^2 < 100000.0	0.0114	283	116

(*b*) In equal reciprocal space volume intervals of $S = \sin\theta/\lambda$.

Interval (Å^{-1})	R	Number of terms	Number of means
0 < S < 0.584	0.0130	720	266
0.584 < S < 0.736	0.0197	875	322
0.736 < S < 0.842	0.0246	737	291
0.842 < S < 0.927	0.0283	637	250
0.927 < S < 0.999	0.0354	508	207
0.999 < S < 1.061	0.0362	419	169
1.061 < S < 1.117	0.0393	387	162
1.117 < S < 1.168	0.0507	335	136
1.168 < S < 1.215	0.0536	279	117
1.215 < S < 1.258	0.0666	266	112
1.258 < S < 1.299	0.0644	240	104
1.299 < S < 1.337	0.0728	250	110
1.337 < S < 1.373	0.0791	225	99
1.373 < S < 1.407	0.0813	204	92
1.407 < S < 1.440	0.0871	144	66
1.440 < S < 1.471	0.1128	166	78
1.471 < S < 1.501	0.1101	113	53
1.501 < S < 1.530	0.1041	119	57
1.530 < S < 1.558	0.0946	41	20
1.558 < S < 1.585	0.3094	2	1

For the chromium complex the dependence of the merging R factors* on the magnitude of the squared structure factors and on the $\sin\theta/\lambda$ interval is given in Table 3. It is especially pleasing that the agreement factors for the strongest reflections are close to 1%, which is as good or better than that achievable with conventional low-temperature diffractometer data. The poorer agreement for the weaker reflections is as expected on the basis of statistical considerations.

To illustrate the quality of the data, we use standard deformation maps calculated directly from the data, with the caveat that the quantitative features may be affected by the omission of the low-order ΔF values. This does not reduce the value of the deformation maps as a criterion for data quality. The low-order data are not essential when aspherical atom least-squares techniques are used, and *model deformation densities* based on the refinement functions are used in the interpretation.

4. Results

4.1. *Sodium nitroprusside (SNP)*

Structural parameters from the study by Pressprich, White, Vekhter & Coppens (1994) were used in the initial

* $R = \sum_{hkl}\sum_{i=1}^{N}|I(hkl)_i - \langle I(hkl)\rangle| / \sum_{hkl}\sum_{i=1}^{N}|I(hkl)_i|$, after conversion to a common scale.

refinements. The deformation density in the plane of the cyano ligands is shown in Fig. 1. No averaging was performed in the calculation of the map. Even though the crystal was larger than optimal, the map is of quite reasonable quality and shows good consistency between the crystallographically independent cyano ligands (the trace of the crystallographic mirror plane at $c = 1/4$, in which the Fe atom is located, runs diagonally across the figure). An aspherical atom refinement was performed using the multipole formalism (Hansen & Coppens, 1978). The static deformation map, based on the least-squares multipole functions, is shown in Fig. 2, whilst the *d*-orbital populations on the iron atom, derived from the least-squares multipole populations (Holladay, Leung & Coppens, 1983), are compared with theoretical Fenske–Hall and multiple-scattering results in Table 4. As observed in other cases, approximate calculations such as Fenske–Hall overestimate the covalency, and therefore the population of the crystal-field destablized orbitals (see, for example, Coppens, 1989). The agreement with the multiple-scattering calculation is much better, with relatively small discrepancies which may be due to deficiencies in either theory or experiment.

4.2. *Hexaamminechromium(III) hexacyanochromate(III)*

This compound was the subject of the first synchrotron charge-density study, performed at room temperature with $\lambda = 0.302$ Å photons (Nielsen, Lee & Coppens, 1986). The present study has the advantage of a much smaller crystal, a low-temperature sample environment, and much more rapid data collection. Deformation-density maps through the plane of the Cr and the four cyano ligands with cut-offs of reflections included of $(\sin\theta/\lambda)_{max} = 0.7$ and 1.0 Å^{-1} are shown in Fig. 3. In terms of noise, shape of the features and peak heights, the maps compare favorably with the published room-temperature maps [with $(\sin\theta/\lambda)_{max} = 0.8$ Å^{-1}] of the earlier synchrotron study. Especially for the nitrogen lone pairs, which are at the periphery of the ion, the peak heights are higher in the present study, undoubtedly due to the reduction in thermal motion. The effect of lowering the temperature is also evident on comparing the cyano group densities in the two compounds reported in this study (Figs. 1 and 3*a*). That the lone-pair scattering persists beyond 0.7 e Å^{-1} is evident from the increase in peak heights on going from Fig. 3(*a*) to Fig. 3(*b*). Maps with $(\sin\theta/\lambda)_{max} = 1.1$ Å^{-1} (not shown) show no significant further increases in the lone pair or bonding regions. The sharp almost spherical features around the Cr atoms are the subject of further study, and thought to be related to the inclusion of very high order data in the least-squares refinements on which the maps are based.

d-Orbital occupancies for the Cr atoms, derived from the multipole population parameters, are listed in Table 5, and for the $[Cr(CN)_6]^{3-}$ ion compared with theoretical values

Table 4
d-Orbital populations of the Fe atom in sodium nitroprusside.

	$d_{x^2-y^2}$	d_{z^2}	$d_{xz} = d_{yz}$	d_{xy}
This study	0.62 (4)	0.32 (6)	1.14 (4)	1.68 (6)
FH*	1.17	1.09	1.36	1.78
Multiple scattering†	0.66	0.56	1.47	1.82

* Fenske–Hall calculation (Pressprich, 1993). † Multiple-scattering calculation (Braga, Pavao & Leite, 1981).

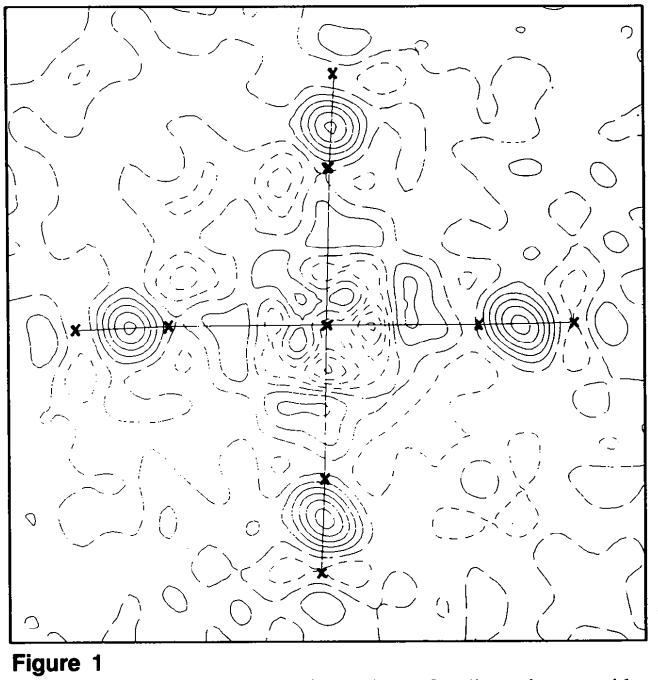

Figure 1
Deformation density in the $Fe(CN)_4$ plane of sodium nitroprusside. Reflections with $\sin\theta/\lambda < 0.7$ Å^{-1} are included. Contours are at 0.1 e Å^{-1}. A crystallographic mirror plane is perpendicular to the section shown. The intersection of the two planes runs diagonally across the picture.

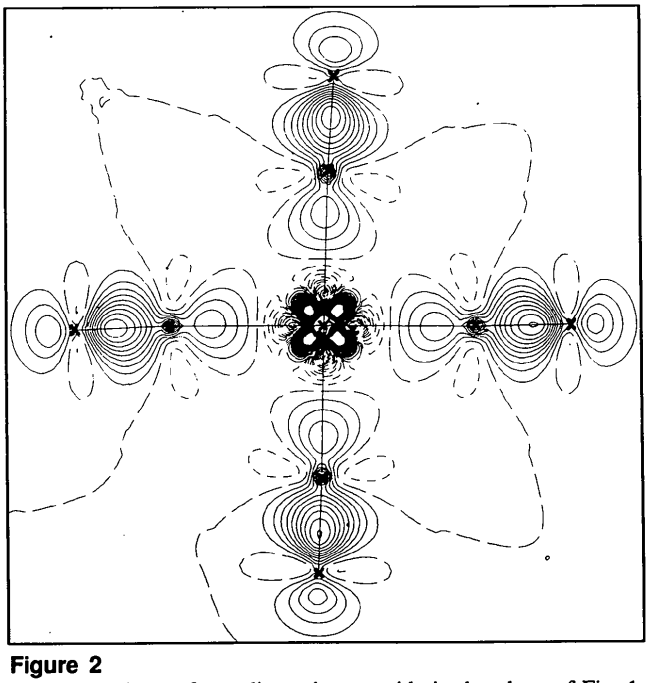

Figure 2
Static model map for sodium nitroprusside in the plane of Fig. 1. Contours are as in Fig. 1.

for the $3d_\sigma$ and $3d_\pi$ (*i.e.* the sum of a_{1g} and e_g) occupancies of Sano, Kashiwagi & Yamatera (1982). The agreement is again satisfactory and trends are the same in both sets of results.

5. Conclusions

We conclude that with imaging plates and the low-temperature technology now available, synchrotron low-temperature data can now be collected with at least the accuracy available with conventional detection devices.

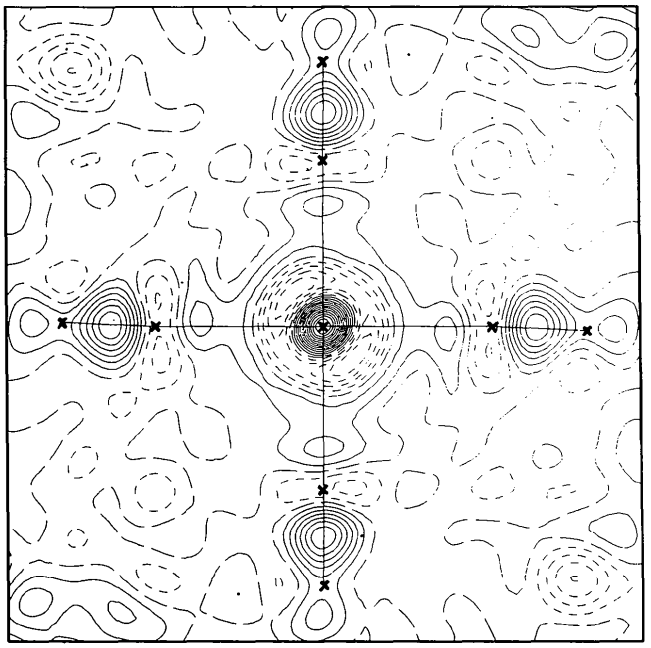

(*a*)

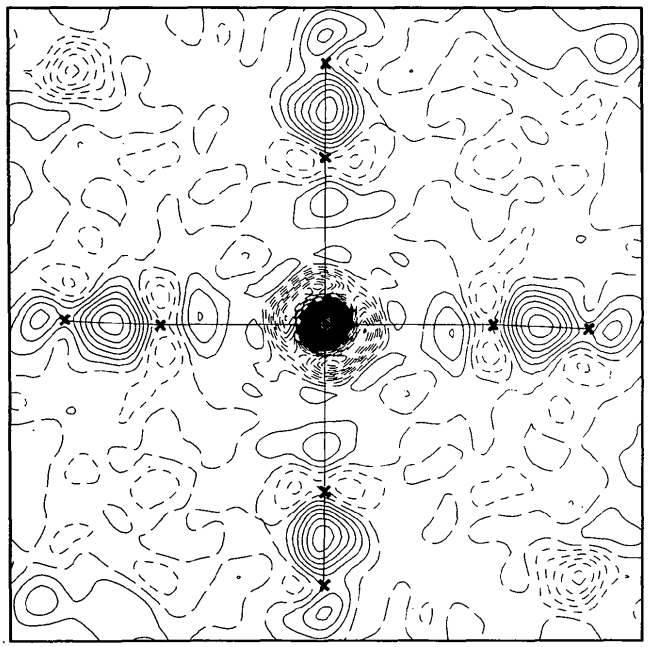

(*b*)

Figure 3
Deformation density in the $Cr(CN)_4$ plane of hexaamminechromium(III) hexacyanochromate(III). Contours are as in Fig. 1. (*a*) $(\sin\theta/\lambda)_{max} = 0.7$ Å^{-1}. (*b*) $(\sin\theta/\lambda)_{max} = 1.0$ Å^{-1}

Table 5
d-Orbital populations of Cr atoms in hexaamminechromium(III) hexacyanochromate(III).

	a_{1g}	e_g	e_g'	$(e_{g+}e_{g+}' + e_{g-}e_{g-}')$*
Cr in $Cr(NH_3)_6$	0.97 (5)	1.50 (7)	0.44 (7)	1.2 (1)
Cr in $Cr(CN)_6$	0.80 (5)	1.59 (8)	0.72 (8)	0.6 (1)
Theory†				
Cr in $Cr(CN)_6$		2.969	0.806	

* Cross term, see Holladay, Leung & Coppens (1983). † SCF-HF (Sano, Kashiwagi & Yamatera, 1982).

Synchrotron radiation has the important advantage of eliminating the $\alpha_1 - \alpha_2$ splittings of the high-order reflections that occur with conventional sources, and allowing the use of very small crystals and short wavelengths. It is clearly the radiation of choice for the rapid collection of accurate data to be used in charge-density analysis.

Support of this work by the National Science Foundation (CHE9021069) is gratefully acknowledged. Research carried out in part at the National Synchrotron Light Source at Brookhaven National Laboratory, which is supported by the US Department of Energy, Division of Materials Sciences and Division of Chemical Sciences. The SUNY X3 beamline at NSLS is supported by the Division of Basic Energy Sciences of the US Department of Energy (DE-FG02-86ER45231).

References

Bolotovsky, R., White, M. A., Darovsky, A. & Coppens, P. (1995). *J. Appl. Cryst.* **28**, 86–95.
Braga, M., Pavao, A. C. & Leite, J. R. (1981). *Phys. Rev. B*, **23**, 4328–4336.
Coppens, P. (1989). *Computational Chemistry – The Challenge of d and f Electrons*, ACS Symposium Series Vol. 394, edited by D. R. Salahub & M. C. Zerner, pp. 39–57. Washington, DC: American Chemical Society.
Darovsky, A., Bolotovsky, R. & Coppens, P. (1994). *J. Appl. Cryst.* **27**, 1039–1040.
Darovsky, A., Meshkovsky, I. & Coppens, P. (1995). *J. Synchrotron Rad.* **2**, 77–78.
Graafsma, H., Sagerman, G. & Coppens, P. (1991). *J. Appl. Cryst.* **24**, 961–962.
Grochowski, J., Serda, P., Wilson, K. S. & Dauter, Z. (1994). *J. Appl. Cryst.* **27**, 722–726.
Hansen, N. K. & Coppens, P. (1978). *Acta Cryst.* A**34**, 909–921.
Holladay, A., Leung, P. C. & Coppens, P. (1983). *Acta Cryst.* A**39**, 377–387.
Iversen, B., Bolotovsky, R., Darovsky, A. & Coppens, P. (1995). In preparation.
Nielsen, F. S., Lee, P. & Coppens, P. (1986). *Acta Cryst.* B**42**, 359–364.
Pressprich, M. R. (1993). Unpublished results.
Pressprich, M. R., White, M. A., Vekhter, Y. & Coppens, P. (1994). *J. Am. Chem. Soc.* **116**, 5233–5238.
Sano, M., Kashiwagi, H. & Yamatera, H. (1982). *Inorg. Chem.* **21**, 3837–3841.
Tan, K., Darovsky, A. & Parise, J. B. (1995). *J. Am. Chem. Soc.* In the press.